THE JOURNAL OF PHYSICAL CHEMISTRY B

Article

pubs.acs.org/JPCB

Highly Ordered Nanorod Assemblies Extending over Device Scale Areas and in Controlled Multilayers by Electrophoretic Deposition

Ajay Singh,[†,§] Niall J. English,[‡] and Kevin M. Ryan*[,†,§]

[†]Materials and Surface Science Institute and Department of Chemical and Environmental Sciences, University of Limerick, Limerick, Ireland

[‡]UCD School of Chemical and Bioprocess Engineering and Centre for Synthesis and Chemical Biology, University College Dublin, Belfield, Dublin 4, Ireland

[§]SFI-Strategic Research Cluster in Solar Energy Research, University of Limerick, Limerick, Ireland

Supporting Information

ABSTRACT: Here we describe the formation of vertically aligned nanorod assemblies over several multilayers using CdS and CdSe nanorods by electrophoretic deposition. The presence of both charge and dipole on the rods allows both field driven deposition and orientational order to form close packed arrays where each rod is vertically aligned. Comparing assembly formation in electrophoresis to spontaneous assembly in solution gives important insights into nanorod organization by these different mechanisms. We show the influence of ligand environment on net charge (zeta potential) and its influence on assembly formation in CdSe nanorods that have long chain alkyl ligands (low charge) or pyridine ligands (high charge). The experimental observations show that highly charged rods deposit too quickly to allow close-packing to occur with perpendicular alignment only occurring with a lower net charge. This is supported by simulation predicting a lower energy configuration with a preference for perpendicular alignment as the charge state decreases. The resolute order that is retained over device scale areas and over several multilayers combined with inherent scalability of electrophoretic deposition makes this approach highly attractive for large scale nanorod integration in electronic, photonic, or photovoltaic devices.

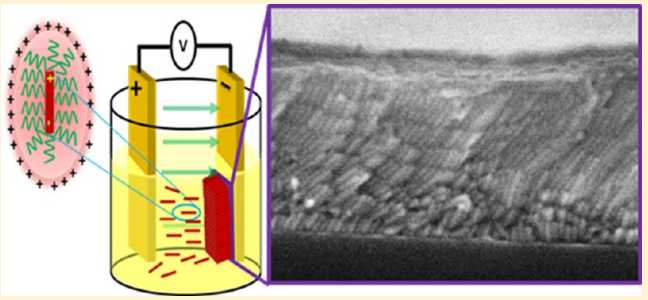

INTRODUCTION

Colloidal nanorods are an important material set where electronic and optical properties are size tunable in both length and diameter and hence controllable.[1−4] Organization of nanorods into assemblies at practical length scales using reproducible protocols is important if their predicted impacts in wide ranging applications from photovoltaics to energy storage are to be realized.[1,5−8] Shape anisotropy in nanorods creates a barrier to rational assembly, although successful approaches in solution have been achieved by addition of external additives either as excess surfactants, polymers, or solvents to induce depletion attraction.[1,5,9−14] Alternatively, external directing agents such as highly oriented pyrolytic graphite or drying under an electric field have been successful over small areas.[15−18] We have recently shown that the net charge and dipole moment on nanorods has a significant influence on their assembly. In the absence of external forces on a solution, the charge dipole interactions have a distance and hence concentration dependence which when optimized allows for spontaneous clustering of the rods into 2D sheets that drop to the surface under gravity sedimentation.[19−22] As these interactions are Coulombic, they can be calculated allowing for predictive control of assembly (whether 1D or 2D) by tuning the net charge through ligand exchange. A limitation is that large area coverage is attained by overlapping of these preformed sheets, leading to a nonuniform construct unsuitable for reproducible application.

Electrophoretic deposition as a viable route to layer formation with colloidal particles is known, yet it is only recently that this approach has been optimized to form assemblies of nanocrystals with a high degree of order at a surface.[23−38] We have shown that electrophoretic deposition is an effective route for the formation of close packed assemblies of both spherical and rod-shaped nanocrystals. The presence of a net charge on the as-synthesized colloidal nanocrystals allowed their controlled deposition.[26] In the case of spherical nanocrystals, the electrophoretic route allowed not just close packed order but localization of assemblies to discrete lithographic trenches.[38] With rods, the charge allowed deposition with the inherent dipole moment due to the noncentrosymmetric wurtzite lattice ensuring orientational order in the final deposit.[39,40] The nanorods were organized

Special Issue: Electrophoretic Deposition

Received: May 28, 2012
Revised: September 19, 2012
Published: October 26, 2012

dx.doi.org/10.1021/jp305184n | J. Phys. Chem. B 2013, 117, 1608−1615

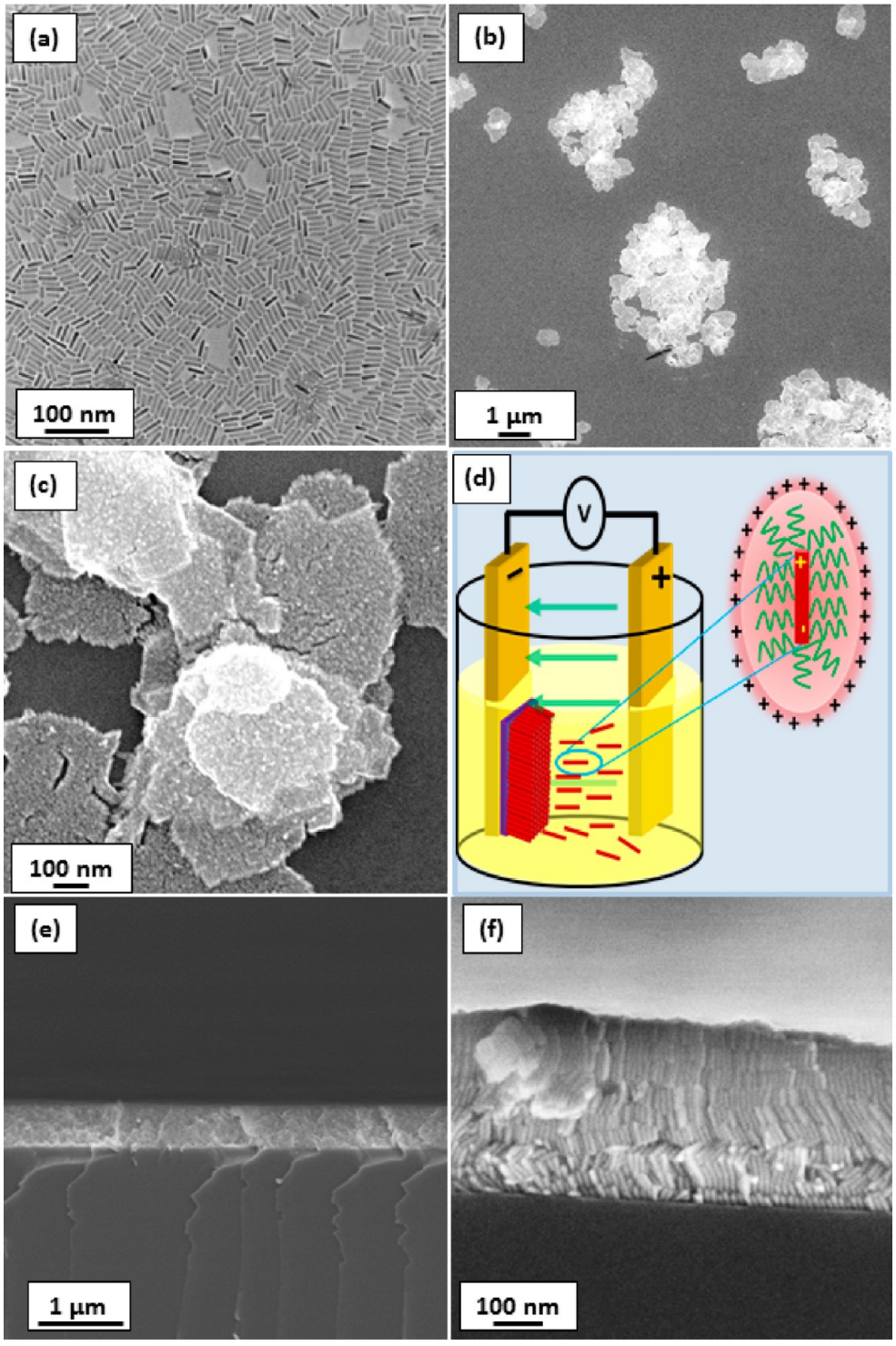

Figure 1. (a) Low-resolution TEM of highly monodispersed CdS nanorods of dimension (7×30 nm^2). (b and c) Low-resolution TEM and SEM images showing the drop-cast assembly of a CdS nanorod. (d) Schematic representation showing the EPD setup. (e and f) Low-resolution and high-resolution SEM cross-section images showing a multilayer vertically aligned CdS nanorod over a large area obtained by electrophoretic deposition.

into close packed assemblies with each rod vertically aligned extending over centimeter scale areas.

Here we expand on this electrophoretic route for nanorod assembly, demonstrating accurate control over the number of nanorod layers deposited on a surface with each layer perfectly aligned and close-packed. We further show the importance of nanorod charge in addition to dipole on the electrophoretic assembly process expanding on interactions in the solution state. We extend the protocol to CdSe and show how differences in charge, dipole, and rod shape in comparison to CdS rods affect the assembly. The as-synthesized rods having a low net charge can be induced to form ordered assemblies, whereas when the charge is dramatically increased by ligand exchange the rods no longer form perfect assemblies. The balance between field driven (electrophoresis) and entropic assembly is discussed in detail with both needed for optimum

dx.doi.org/10.1021/jp305184n | J. Phys. Chem. B 2013, 117, 1608−1615

ordering in the array. A theoretical treatment of assembly correlates well with the experimental results, confirming that field driven effects are dominant in solution to push the nanocrystals to the surface with entropic considerations manifesting to allow close-packing at the interface.

EXPERIMENTAL SECTION

Materials. Cadmium oxide (>99%), trioctylphosphine (TOP, 90%), tri-*n*-octylphosphine oxide (TOPO, 99%), sulfur (99.98%), and selenium (99.98%) were purchased from Aldrich. *n*-Octadecylphosphonic acid (ODPA), *n*-tetradecylphosphonic acid (TDPA), and *n*-hexylphosphonic acid (HPA) were obtained from PolyCarbon Industries, Inc. (PCI). All the chemicals were used as received.

Synthesis of CdS Nanorods. CdS nanorods were synthesized according to previously published methods in an inert atmosphere using standard air free techniques.[3,4] In detail, 0.21 g of CdO, 1.08 g of ODPA, and 2.73 g of TOPO were loaded into a 25 mL three-neck flask and heated to 120 °C under argon gas flow at which CdO, ODPA, and TOPO were dissolved. The mixture is further evacuated at 120 °C for 20 min with a vacuum range of 150−200 mTorr to remove any impurities and moisture (first degas). Next, the mixture is ramped to 300 °C under argon flow at which CdO completely dissolves and the solution becomes optically clear. The solution is cooled to 120 °C and further degassed for another 45 min. After this second degas, the mixture was heated to 310 °C under argon flow at which sulfur stock solution (∼800 μL) containing 64 mg of sulfur in 7.64 mg of TOP is rapidly injected and nanocrystals were allowed to grow for 30 min before removal of the heating mantle. When the temperature reached ∼80 °C, the reaction was quenched via the addition of 2−3 mL of anhydrous toluene. The nanorods were purified by 3−4 times by dissolution in toluene and precipitation from acetone.

Synthesis of CdSe Nanorods. CdSe nanorods were also synthesized in a procedure similar to that of CdS nanorods. Briefly, CdO (0.20 g), *n*-tetradecylphosphonicacid (TDPA, 0.71g), *n*-hexylphosphonic acid (HPA, 0.16g), and tri-*n*-octylphosphine oxide (TOPO, 3.00g) were placed in a three-neck flask equipped with a condenser and a thermocouple adapter. The mixture was heated to 120 °C in an atmosphere of Ar and then evacuated for 1 h. The mixture was further heated up to 300 °C under an argon atmosphere so that CdO decomposed and gave an optically clear solution. Once a clear solution was achieved, 1.5 g of trioctylphosphine (TOP) was added to the mixture, and the temperature was further raised to 310 °C. Next, selenium (∼500 μL) stock solution was injected rapidly, containing 73 mg of selenium in 416 mg of TOP, and the resulting nanocrystals were further allowed to grow for 5−10 min at 310 °C. The growth of nanorods was terminated by removal of the heating mantle, and at 80 °C, 2−4 mL of anhydrous toluene was added to the mixture to quench the reaction. The nanorods were washed three times in a 1:1 toluene:isoproponal mix to remove any excess surfactants.

Electrophoretic Deposition. A toluene solution of CdSe (5% w/v) and CdS nanorods (10% w/v) was used for deposition. Prior to deposition, the nanorod solution was sonicated for 5−10 min to achieve good dispersion of nanorods in toluene. During deposition, the silicon substrates (10 mm × 10 mm) were attached onto the negative electrodes, of two parallel gold coated copper electrodes separated at 2 mm apart. The electrodes were completely immersed in a nanorod solution, and a potential of 200 V was applied to the substrate for 3 min using a high voltage power supply unit (TECHNIX SR-5-F-300, S/N: BU08/04971), where voltage was monitored using a Black star 3225 MP millimeter. After deposition, the electrodes were pulled out from the nanorod solution bath and dried slowly. The silicon substrate is put in the desiccator to remove all solvent before further characterization.

Ligand Exchange (Pyridine) of CdSe Nanorods. For ligand exchange of CdSe nanorods with pyridine, 1 mL of as-synthesized CdSe nanorod solution was dispersed in anhydrous pyridine (5−7 mL) followed by vortex for 10 min and then sonicated for 30−45 min. The solution then was centrifuged at 13 000 rpm for 10−15 min. The filtrate was discarded, and the resulting nanorod was redispersed in toluene.

Analysis. The as-synthesized CdS and CdSe nanorods imaged on Cu coated TEM grids are characterized by transmission electron microscopy (TEM) by using a JEOL JEM-2011F instrument operating at an accelerating voltage of 200 kV. Scanning electron microscopy (SEM) of the nanorod assembly on a Si(111) substrate was performed with a Hitachi S-4800 machine. Zeta-potential was measured using a Zeta PALS (Zeta Potential Analyzer, Brookhaven Instruments Corporation, US) using low and high electric field, E = 137 and 274 V cm^{-1}, across the palladium electrodes, and the measured zeta-potential values were constant from two fields which were averaged from 10 repeated experiments. The X-ray diffractograms analysis was carried out on a PANalytical X'Pert MPD Pro using Cu Kα radiation with a 1-D X'Celerator strip detector.

RESULTS AND DISCUSSION

There are a multitude of influential factors to be considered when nanorod assembly is investigated in solution. The physical properties of the rod such as size, shape, net charge, dipole moment, and ligand environment are significant. A low degree of polydispersity in rod length and diameter is a necessary prerequisite if close packed ordering is to be attained. While the dipole moment is inherent to the crystallographic structure (noncentrosymmetric wurtzite lattice in the case of rods), the remaining physical properties are largely controllable through repeated synthetic optimization. Figure 1a shows a TEM image of CdS nanorods (7 × 30 nm^2) with a very low polydispersity that are routinely achievable. In a solution of these rods, the strongest rod−rod interactions are Coulombic, meaning a distance and hence concentration dependence determines whether assembly occurs spontaneously in solution or dispersion is maintained. Modulating the concentration of the rods in part a results in their spontaneous assembly into discs that drop to the surface under gravity sedimentation (b and c). As the ligand capped rods are designed to be solubilized in organic solutions, the nature of the solvent interaction is also important with solubility (dispersibility of the rods), volatility, viscosity, and polarity all contributing either positively or negatively to the resultant assembly. For example, the screening effect of the solvents on the Coulombic interactions needs to be considered in determining the optimum assembly protocol. The presence and influence of unwanted impurities in this solvent, particularly excess surfactant, is often overlooked but can be highly detrimental to assembly formation if not controlled. Under the influence of an electric field, all of these factors are equally relevant, although the driving force for assembly is clearly different. Advances in understanding of the kinetics of electrophoretic deposition allow correlation of the

dx.doi.org/10.1021/jp305184n | J. Phys. Chem. B 2013, 117, 1608−1615

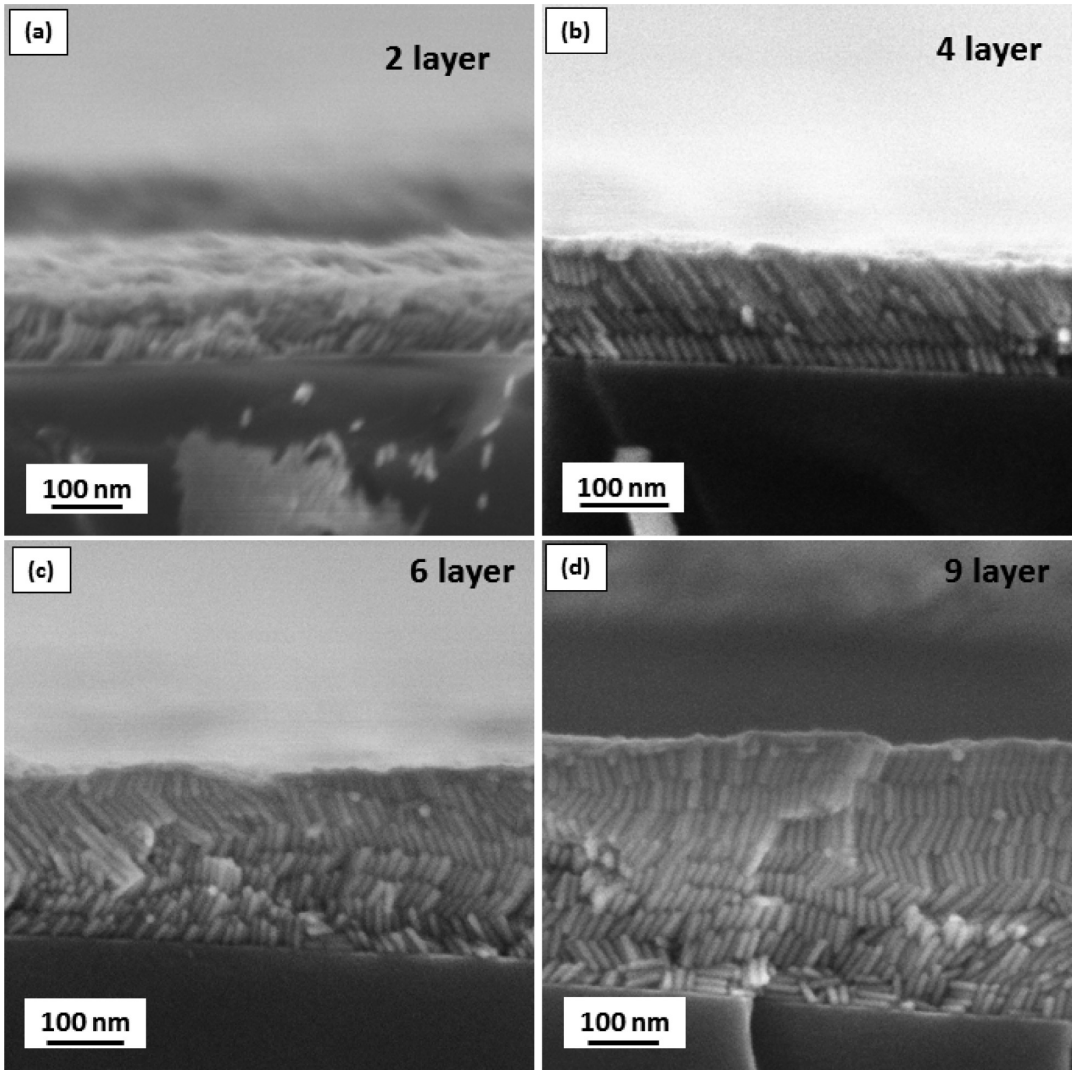

Figure 2. SEM images showing the control on number of layers with respect to deposition time from 30, 60, 120, and 180 s.

properties of the colloidal suspension such as concentration and zeta potential to the external factors of field strength, deposition area, and deposition time. In our studies, we work in a normalized system with equally sized flat planar electrodes (Figure 1d) and toluene as a solvent.

Toluene has a low dielectric constant (ϵr = 2.38) and a viscosity of (0.56), resulting in relatively low electrophoretic mobilities in comparison to higher dielectric solvents such as water. We have previously shown that the charge is influenced by the structure of the coordinating ligand with 8 nm × 100 nm CdS nanorods having a zeta potential of ∼50 mV and organizing into perpendicular arrays under electrophoresis. The shorter aspect ratio rods, Figure 1a, have a zeta potential of 9 ± 5 mV which is the expected charge reduction as the surface area decreases given the previously determined influence of ligand on the charge state. This approximates to similar mobility values given the proportional reduction in volume (hydrodynamic radius). Under similar assembly conditions (200 V, parallel electrodes 1 cm apart), highly ordered close packed arrays are obtained with each rod vertically aligned. The LRSEM image in Figure 1e and HRSEM image in Figure 1f are cross-section images of centimeter scale deposits showing the extraordinarily resolute order throughout the layer. In Figure 1f, the perfect axial alignment and close packing in each layer is evident with rods spaced at ∼2 nm by the ligand spacers. In contrast to our previous reports, no additional surfactant deposits between the layers such that the film thickness is an exact multiple of the rod lengths.[35] This was achieved by carrying out sufficient antisolvent precipitations of the as-synthesized solution to remove all organic material except for ligands directly bound to the rods. This resolute assembly at a substrate interface would not be possible in non-field-driven approaches and demonstrates the effectiveness of EPD for thin-film formation from nanorod suspensions. Extending the deposition time to 30, 60, 120, and 180 s allows the number of layers to be accurately controlled with 2, 4, 6, and 9 sequential layers of rods attained, as seen in Figure 2. Importantly, no loss of ordering is observed when subsequent layers are deposited on preformed layers, indicating that each layer formed acts as a planar surface for the next depositing layer. The close packing of the rods is interesting, as this will only occur in a dynamic situation with a rod finding its preferred location on the deposit before locking in. This strongly suggests that, whereas the particle migration to the electrodes is field driven, interparticle forces are dominating at the interface to allow the lowest potential energy (close packing) of the final deposit to be reached. This is in good agreement with similar evaluations of potential energy

dx.doi.org/10.1021/jp305184n | J. Phys. Chem. B 2013, 117, 1608−1615

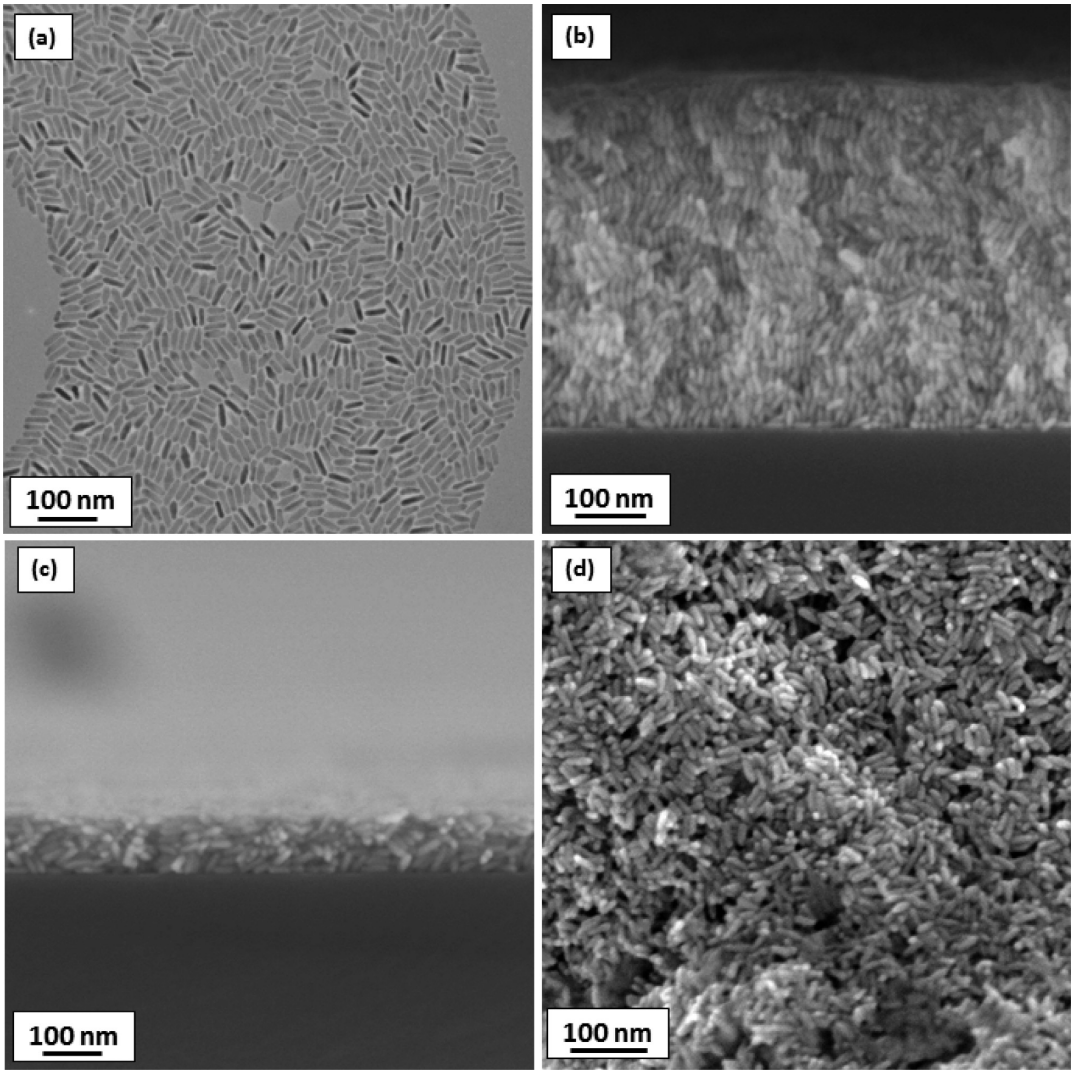

Figure 3. (a) TEM image showing the rice-shape CdSe nanorod. (b) SEM cross-section image showing a multilayer vertical assembly of a CdSe nanorod. (c and d) SEM images showing the cross-section and top down image of randomly lying pyridine washed CdSe nanorod where no preferential ordering is seen.

interactions with spherical nanocrystals under EPD reported by Dickerson.[41]

Extension of EPD deposition to CdSe nanorods was evaluated to show the general applicability of this system. CdSe nanorods are typically rice-shaped in comparison to the perfect columnar shape of CdS and are therefore more difficult to assemble in general (Figure 3a). The as-synthesized rods are capped in phosphonates/TOPO and after several washings show a zeta potential of ~5 mV with an aspect ratio of 3. The reduction in net charge is again consistent with the reduced surface area of the rice shape and will again result in comparable mobilities to the CdS rods given the associated volume reduction. The rods have a low barrier to aggregation in solution, and the optimum conditions for EPD required a lower concentration under 200 V to achieve assembly. Figure 3b shows a cross-sectional SEM image of the resulting deposit after 5 min deposition. Again, the rods are vertically aligned in the deposit with areas of side by side ordering although not as resolute as the CdS rods. This can be largely attributed to the rice shape being inherently less suitable for close packing in two or three dimensions. The conservation of vertical orientation with comparable density of packing is important, as these materials are important photoabsorbers and this EPD route is an ideal low cost replacement for expensive vacuum processes.[1,3] When the ligands are exchanged for pyridine, the zeta potential dramatically increases to ~35 mV. EPD of these rods leads to disordered assemblies at the substrate regardless of solution concentration (Figure 3c,d). The increased charge will correlate with an order of magnitude increase in electrophoretic mobility, resulting in deposition of the particles to the surface at a rate that prevents interparticle forces and/or entropic considerations to allow the lowest potential energy state of the final deposit to be reached. Lowering the voltage does increase the order (Supporting Information, Figure S3), although the deposition time becomes a limiting factor for practical application. Further characterization of large scale assemblies of both unaligned and aligned nanorods was carried out using X-ray powder diffraction (see details in Supporting Information, Figure S4). In the aligned nanorod sample, only a single peak corresponding to the (002) plane is observed consistent with all rods being oriented along a single crystallographic direction.

To further elucidate the influence of charge on assembly formation, we performed nonequilibrium MD simulations of

dx.doi.org/10.1021/jp305184n | J. Phys. Chem. B 2013, 117, 1608−1615

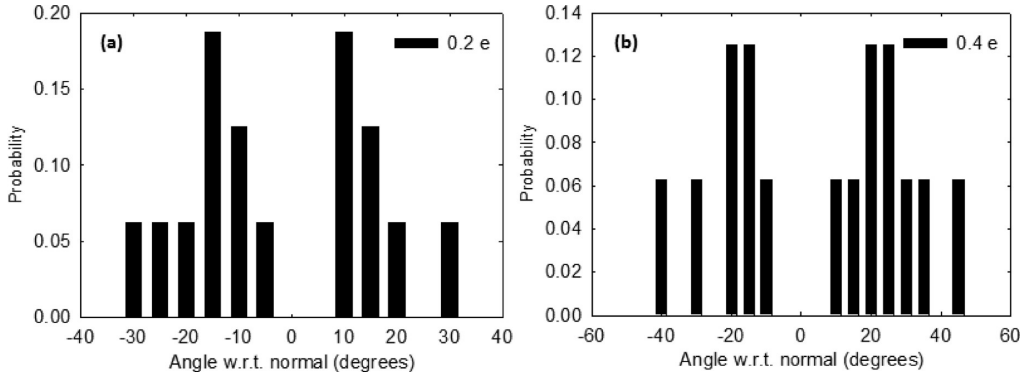

Figure 4. Normalized probability distribution of the rods' axes vis-à-vis the normal to the surface for the (a) 0.2e-charged rods and (b) 0.4e-charged rods.

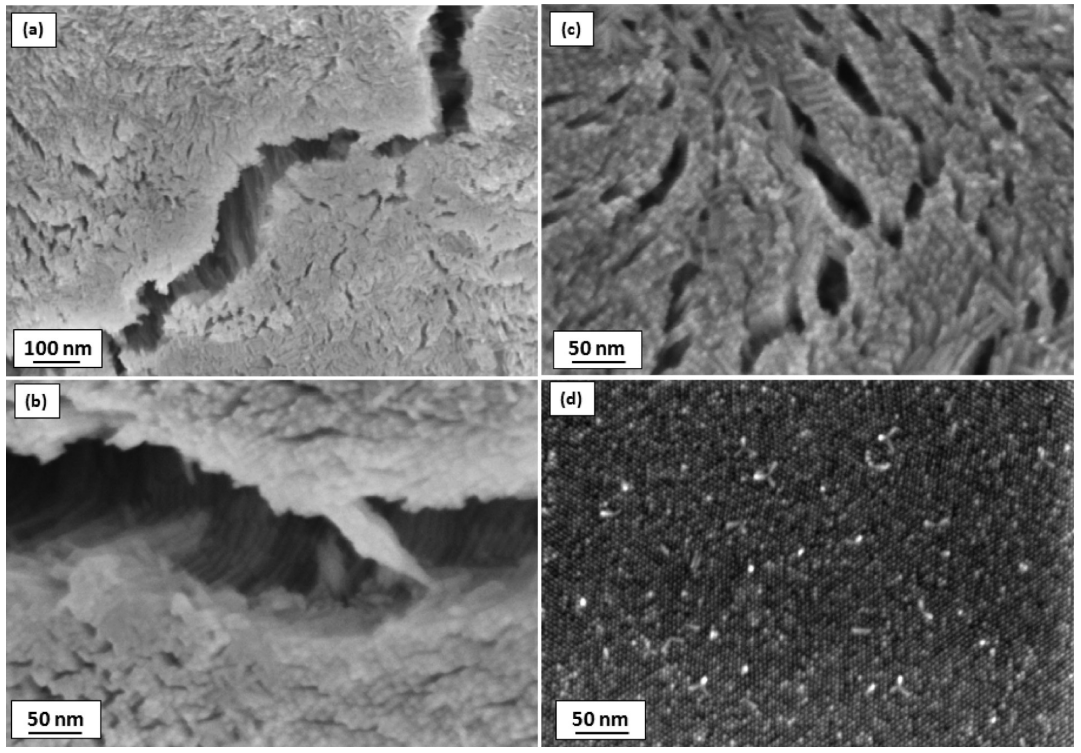

Figure 5. SEM images showing the effect of solvent drying on deposited nanorod film.

EPD to obtain molecular level insights to approximate the experimental results.[42−45] Two charge states (0.2e, 0.4e) were applied to small, charged CdSe nanorods (18 Å in height and 5 Å in diameter, comparable aspect ratio to experimental scaled to allow for limitations of model). The EPD simulation was carried out in external electric fields E of 0.03 V/Å in the z-direction in toluene (Supporting Information for full simulation methodology and background). Once deposition was complete, it was found that the rods remained relatively stable in situ with the energy of the deposited system for the 0.2e-charged rods lower than that of their more highly charged counterparts. The postdeposition probability distributions of the orientation angles of the rods' axes with respect to the surface-normal are shown in Figure 4. For the 0.2e-charged rods, the slower deposition affords greater scope for a greater extent of dipolar rotational alignment with the applied field vis-à-vis the 0.4e surface-charge case. Therefore, there is a greater likelihood of more perpendicular alignment to the surface (i.e., a smaller absolute value of the angle relative to the surface normal) once deposited; quantitatively, the likelihood was found to be about 70% within ±20° for the 0.2e case, as compared to around 30% within this range for the 0.4e scenario. While this model is highly idealized, it does confirm the experimental finding in relation to the effect of charge, dipole, and deposition speed on ordering in the final deposit. The lower energy consideration of the more slowly deposited rods suggests that entropy driven crystallization does play an important role in the formation of ordered arrays by electrophoretic deposition.

After EPD, the removal of the substrate from the solvent can lead to drying induced cracking in the deposited layer. This is a well-known phenomenon that occurs when trapped solvent molecules evaporate, causing intrinsic strain and stress as the distance between the particles decreases.[28] Figure 5a,b shows examples of cracks propagating in a rapidly dried CdS nanorod film. The cracks propagate laterally and to a depth of several multilayers, as evident in the higher magnification image (5c).

dx.doi.org/10.1021/jp305184n | J. Phys. Chem. B 2013, 117, 1608−1615

The absence of delamination between the layers shows that the end−end and side−side packing is still conserved with random cleavage along the interdigitated surfactant between rods where the greatest strain is accumulated. If the electrodes are dried very slowly in the saturated solvent vapor atmosphere (Supporting Information, Figure S5), the cracking is eliminated (Figure 5d). The organic ligand does play a role in accommodating the strain under controlled evaporation conditions such that ligand coverage, ligand length, and film thickness are influencing factors on the formation of defect free deposits.

CONCLUSIONS

EPD of semiconductor nanorods from toluene allows their deposition into close packed layers with resolute vertical alignment extending over device scale areas. In sequential multilayers, the perpendicular order is conserved with up to nine layers shown with the number of layers controlled by the deposition time. The extension of EPD from CdS to CdSe is successfully demonstrated where, although the ligand environment is different, the similar mobilities allow assembly formation with the retention of vertical alignment. The shape of the particle is further shown to have an influence on the final deposit with the rice-shaped CdSe not allowing for a similar degree of end-to-end order as achieved with the CdS. The influence of net charge on the assembly is outlined for the first time where after a pyridine wash the higher charged CdSe no longer assembles, as the deposition is too fast to allow the lowest energy consideration to be reached. This is confirmed by simulation of a model system of rod deposition in toluene where net charge and relative deposition rates are shown to impact the rod ordering and hence the energy consideration attainable. The effect of solvent evaporation on crack propagation shows similar behavior to spherical nanocrystal assemblies with conformal deposits attained by drying in a solvent rich environment. The results show the effectiveness of EPD for the creation of highly ordered nanorod assemblies at length scales amenable to real application with outstanding possibilities for photovoltaic and photoemission devices.

ASSOCIATED CONTENT

Supporting Information

Details of the simulation methodology and procedure, photograph of the substrate after deposition, XRD analysis of assembly, photograph showing the electrode drying process in solvent saturation environment, and assembly of a ligand exchange nanorod with EPD. This material is available free of charge via the Internet at http://pubs.acs.org.

AUTHOR INFORMATION

Corresponding Author

*E-mail: Kevin.M.Ryan@ul.ie.

Notes

The authors declare no competing financial interest.

ACKNOWLEDGMENTS

This work was supported principally by Science Foundation Ireland (SFI) under the Principal Investigator Program under Contract No. 11PI-1148 and also by the Advanced Biomimetic Materials for Solar Energy Conversion Strategic Research Cluster (contract 07/SRC/B1160). N.J.E. acknowledges the provision of high performance computing resources provided by Science Foundation Ireland. This work was also conducted under the framework of the INSPIRE programme, funded by the Irish Government's Programme for Research in Third Level Institutions, Cycle 4, National Development Plan 2007−2013.

REFERENCES

(1) Krahne, R.; Morello, G.; Figuerola, A.; George, C.; Deka, S.; Manna, L. *Phys. Rep.* **2011**, *501*, 75−221.
(2) Hu, J.; Li, L.-S.; Yang, W.; Manna, L.; Wang, L.-W.; Alivisatos, A. P. *Science* **2001**, *292*, 2060−2063.
(3) Gur, I.; Fromer, N. A.; Geier, M. L.; Alivisatos, A. P. *Science* **2005**, *310*, 462−465.
(4) Peng, Z. A.; Peng, X. G. *J. Am. Chem. Soc.* **2001**, *123*, 183−184.
(5) Liu, K.; Zhao, N. N.; Kumacheva, E. *Chem. Soc. Rev.* **2010**, *40*, 656−671.
(6) Sanyal, A.; Bala, T.; Ahmed, S.; Singh, A; Piterina, A. V.; McGloughlin, T. M.; Laffir, F. R.; Ryan, K. M. *J. Mater. Chem.* **2009**, *19*, 8974−8981.
(7) Gonzalez-Valls, I.; Lira-Cantu, M. *Energy Environ. Sci.* **2009**, *2*, 19−34.
(8) Amirav, L.; Alivisatos, A. P. *J. Phys. Chem. Lett.* **2011**, *1*, 1051−1054.
(9) Baranov, D.; Fiore, A.; van Huis, M.; Giannini, C.; Falqui, A.; Lafont, U.; Zandbergen, H.; Zanella, M.; Cingolani, R.; Manna, L. *Nano Lett.* **2010**, *10*, 743−749.
(10) Baker, J. L.; Widmer-Cooper, A.; Toney, M. F.; Geissler, P. L.; Alivisatos, A. P. *Nano Lett.* **2010**, *10*, 195−201.
(11) Rivest, J. B.; Swisher, S. L.; Fong, L.-K.; Zheng, H.; Alivisatos, A. P. *ACS Nano* **2011**, *5*, 3811−3816.
(12) Hung, A. M.; Oh, T.; Cha, J. N. *Nanoscale* **2012**, *4*, 1016−1020.
(13) Kang, C. C.; Lai, C. W.; Peng, H. C.; Shyue, J. J.; Chou, P. T. *ACS Nano* **2008**, *2*, 750−756.
(14) Zanella, M.; Gomes, R.; Povia, M.; Giannini, C.; Zhang, Y.; Riskin, A.; van Bael, M.; Hens, Z.; Manna, L. *Adv. Mater.* **2011**, *23*, 2205−2209.
(15) Ahmed, S.; Ryan, K. M. *Nano Lett.* **2007**, *7*, 2480−2485.
(16) O'Sullivan, C.; Ahmed, S.; Ryan, K. M. *J. Mater. Chem.* **2008**, *18*, 5218−5222.
(17) Ryan, K. M.; Mastroianni, A.; Stancil, K. A.; Liu, H. T.; Alivisatos, A. P. *Nano Lett.* **2006**, *6*, 1479−1482.
(18) Carbone, L.; Nobile, C.; De Giorgi, M.; Della Sala, F.; Morello, G.; Pompa, P.; Hytch, M.; Snoeck, E.; Fiore, A.; Franchini, I. R.; et al. *Nano Lett.* **2007**, *7*, 2942−2950.
(19) Singh, A.; Gunning, R. D.; Sanyal, A.; Ryan, K. M. *Chem. Commun.* **2010**, *46*, 7193−7195.
(20) Singh, A.; Gunning, R. D.; Ahmed, S.; Barrett, C. A.; English, N. J.; Garate, J.-A.; Ryan, K. M. *J. Mater. Chem.* **2012**, *22*, 1562−1569.
(21) Singh, A.; Dickinson, C.; Ryan, K. M. *ACS Nano* **2012**, *6*, 3339−3345.
(22) Singh, A.; Geaney, H.; Laffir, F.; Ryan, K. M. *J. Am. Chem. Soc.* **2012**, *134*, 2910−2913.
(23) Giersig, M.; Mulvaney, P. *J. Phys. Chem.* **1993**, *97*, 6334−6336.
(24) Islam, M. A.; Herman, I. P. *Appl. Phys. Lett.* **2002**, *80*, 3823−3825.
(25) Islam, M. A.; Xia, Y.; Telesca, D. A.; Steigerwald, M. L.; Herman, I. P. *Chem. Mater.* **2004**, *16*, 49−54.
(26) Jia, S.; Banerjee, S.; Herman, I. P. *J. Phys. Chem. C* **2008**, *112*, 162−171.
(27) Islam, M. A.; Xia, Y. Q.; Steigerwald, M. L.; Yin, M.; Liu, Z.; O'Brien, S.; Levicky, R.; Herman, I. P. *Nano Lett.* **2003**, *3*, 1603−1606.
(28) Jia, S.; Banerjee, S.; Lee, D.; Bevk, J.; Kysar, J. W.; Herman, I. P. *J. Appl. Phys.* **2009**, *105*, 103513.
(29) Krejci, A. J.; Gonzalo-Juan, I.; Dickerson, J. H. *ACS Appl. Mater. Interfaces* **2011**, *3*, 3611−3615.
(30) Smith, N. J.; Emmett, K. J.; Rosenthal, S. J. *Appl. Phys. Lett.* **2008**, *93*, 043504.
(31) Grinis, L.; Dor, S.; Ofir, A.; Zaban, A. *J. Photochem. Photobiol., A* **2008**, *198*, 52−59.

(32) Mahajan, S. V.; Kavich, D. W.; Redigolo, M. L.; Dickerson, J. H. *J. Mater. Sci.* **2006**, *41*, 8160−8165.
(33) Hasan, S. A.; Kavich, D. W.; Mahajan, S. V.; Dickerson, J. H. *Thin Solid Films* **2009**, *517*, 2665−2669.
(34) Mahajan, S. V.; Dickerson, J. H. *Nanotechnology* **2010**, *21*, 145704.
(35) Ahmed, S.; Ryan, K. M. *Chem. Commun.* **2009**, 6421−6423.
(36) Kelly, D.; Singh, A.; Barrett, C. A.; O'Sullivan, C.; Coughlan, C.; Laffir, F. R.; O'Dwyer, C.; Ryan, K. M. *Nanoscale* **2011**, *3*, 4580−4583.
(37) Singh, A.; Coughlan, C.; Laffir, F.; Ryan, K. M. *ACS Nano* **2012**, *6*, 6977−6983.
(38) Ahmed, S.; Ryan, K. M. *Adv. Mater.* **2008**, *20*, 4745−4750.
(39) Li, L.-S.; Alivisatos, A. P. *Phys. Rev. Lett.* **2003**, *90*, 097402.
(40) Nann, T.; Schneider, J. *Chem. Phys. Lett.* **2004**, *384*, 150−152.
(41) Dickerson, J. H.; Boccaccini, A. R. *Electrophoretic Deposition of Nanomaterials*; Springer: New York, 2012.
(42) Ma, J.; Wang, C.; Liang, C. H. *Mater. Sci. Eng., C* **2007**, *27*, 886−889.
(43) English, N. J.; Long, W. F. *Physica A* **2009**, *388*, 4091−4096.
(44) Garate, J.-A.; English, N. J.; Singh, A.; Ryan, K. M.; MacElroy, J. M. D.; Mooney, D. A. *Langmuir* **2011**, *27*, 13506−13513.
(45) Rabani, E. *J. Chem. Phys.* **2002**, *116*, 258−262.